inorganics

MDPI

Article

New Coordination Polymers of Zinc(II), Copper(II) and Cadmium(II) with 1,3-Bis(1,2,4-triazol-4-yl)adamantane

Nertil Xhaferaj [1,2], Aurel Tăbăcaru [3,*], Marco Moroni [4], Ganna A. Senchyk [5], Kostiantyn V. Domasevitch [5], Claudio Pettinari [2,6] and Simona Galli [4,7,*]

1 Department of Food Technology, Faculty of Food and Biotechnology, Agricultural University of Tirana, Kodër Kamëz, SH1, 1000 Tirana, Albania; nertil.xhaferaj@gmail.com
2 School of Pharmacy, University of Camerino, Via S. Agostino 1, 62032 Camerino, Italy; claudio.pettinari@unicam.it
3 Department of Chemistry, Physics and Environment, Faculty of Sciences and Environment, "Dunarea de Jos" University of Galati, 111 Domneasca Street, 800201 Galati, Romania
4 Dipartimento di Scienza e Alta Tecnologia, Università deli Studi dell'Insubria, Via Valleggio 11, 22100 Como, Italy; mmoroni@studenti.uninsubria.it
5 Inorganic Chemistry Department, Taras Shevchenko National University of Kyiv, 64 Volodimirska Street, 01033 Kyiv, Ukraine; senchyk.ganna@gmail.com (G.A.S.); dk@univ.kiev.ua (K.V.D.)
6 Istituto di Chimica dei Composti Organometallici (ICCOM-CNR), Via Madonna del Piano 10, 50019 Sesto Fiorentino, Italy
7 Consorzio Interuniversitario Nazionale per la Scienza e Tecnologia dei Materiali, Via Giusti 9, 50121 Firenze, Italy
* Correspondence: aurel.tabacaru@ugal.ro (A.T.); simona.galli@uninsubria.it (S.G.)

Received: 16 October 2020; Accepted: 30 October 2020; Published: 6 November 2020

Abstract: The new coordination polymers (CPs) $[Zn(tr_2ad)Cl_2]_n$, $\{[Cu(tr_2ad)Cl]Cl{\cdot}4H_2O\}_n$, $[Cd_2(tr_2ad)Cl_4]_n$, $\{[Cu(tr_2ad)(NO_3)](NO_3)\}_n$ and $\{[Cd(tr_2ad)(NO_3)](NO_3){\cdot}H_2O\}_n$ were obtained in the form of air- and moisture-stable microcrystalline powders by the solvothermal reactions of zinc(II), copper(II) and cadmium(II) chlorides or nitrates with the ligand 1,3-bis(1,2,4-triazol-4-yl)adamantane (tr_2ad). Investigation of the thermal behaviour assessed the thermal stability of these CPs, with $[Cd_2(tr_2ad)Cl_4]_n$ starting to decompose only around 365 °C. As retrieved by powder X-ray diffraction, while $[Zn(tr_2ad)Cl_2]_n$ features 1-D chains along which the metal centre shows a tetrahedral geometry and the spacer is exo-bidentate, the other CPs contain 2-D double-layers in which the metal ions possess an octahedral stereochemistry and the linker is exo-tetradentate. A comparative structural analysis involving known coordination compounds containing the tr_2ad ligand enabled us to disclose (i) the versatility of the ligand, as far as the coordination modes are concerned; (ii) the variability in crystal structure dimensionality, ranging from 1-D to 3-D; (iii) the fact that, to the best of our knowledge, $[Zn(tr_2ad)Cl_2]_n$ is the first Zn^{II}-based CP containing the tr_2ad spacer.

Keywords: coordination polymers; poly(azolate) spacers; 1,3-bis(1,2,4-triazol-4-yl)adamantane; zinc; copper; cadmium; crystal structure

1. Introduction

Since the discovery that metal ions and organic ligands can act as connectors and spacers, respectively, to generate infinite frameworks [1], the chemistry of coordination polymers (CPs) [2–5], including the subclass of metal–organic frameworks (MOFs) [6–10], has recorded a rapid growth, due to the plethora of functional properties they were found to possess. One of the main advantages of CPs

and MOFs is the possibility to modulate their chemical composition, crystal structure and functional properties through a modification of the metal ion and/or the organic spacer. In view of their potential applications, CPs and MOFs appear as interesting platforms which may offer sustainable solutions in fields of major economical, technological and environmental importance, e.g., gas storage and separation [11], catalysis [12], luminescence [13,14], conductivity [15], magnetism [16], sensing [17–19] and biomedicine [20]. The successful preparation of CPs has generally relied on organic ligands from the class of poly(carboxylic) acids [21–23], pyrazines and bipyridines [21–24], phosphonic acids [25] and poly(azoles) [26–28].

Among the nitrogen-donor ligands from the class of poly(azoles), attention has been paid also to 1,2,4-triazolyl derivatives, due to their electron-donating ability and rich coordination chemistry. As a representative example, they can provide the N^1,N^2-bridging between two adjacent metal ions [29] in the same manner as pyrazolates do [30]. Based on the coordination modes they can adopt, 1,2,4-triazolyl ligands have been exploited in building up polynuclear and polymeric coordination compounds [31–35]. This is also the case of the ditopic ligand 1,3-bis(1,2,4-triazol-4-yl)adamantane (tr_2ad, Scheme 1) which, although at present less explored, provides an attractive platform for crystal engineering.

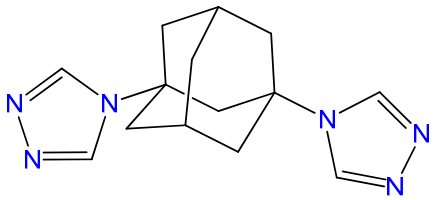

Scheme 1. Molecular structure of 1,3-bis(1,2,4-triazol-4-yl)adamantane (tr_2ad).

Aiming at enlarging and diversifying the library of tr_2ad-based coordination frameworks, we report hereafter on the synthesis, thermal behavior and structural characterization of the five new compounds $[Zn(tr_2ad)Cl_2]_n$, $\{[Cu(tr_2ad)Cl]Cl{\cdot}4H_2O\}_n$, $[Cd_2(tr_2ad)Cl_4]_n$, $\{[Cu(tr_2ad)(NO_3)](NO_3)\}_n$ and $\{[Cd(tr_2ad)(NO_3)](NO_3){\cdot}H_2O\}_n$. The crystal and molecular structures of the anhydrous and trihydrate tr_2ad ligand are also described.

2. Results and Discussion

2.1. Synthesis and Preliminary Characterization

A detailed description of the synthesis of the tr_2ad ligand, including analytical details on the intermediates never reported before, is provided in the Supporting Information.

Several screening reactions, involving the adoption of synthetic conditions differing in solvent, metal-to-ligand ratio, temperature, and/or time, were carried out in order to successfully obtain microcrystalline batches of the tr_2ad-based CPs $[Zn(tr_2ad)Cl_2]_n$, $\{[Cu(tr_2ad)Cl]Cl{\cdot}4H_2O\}_n$, $[Cd_2(tr_2ad)Cl_4]_n$, $\{[Cu(tr_2ad)(NO_3)](NO_3)\}_n$ and $\{[Cd(tr_2ad)(NO_3)](NO_3){\cdot}H_2O\}_n$. Scheme 2 shows the synthetic conditions fruitfully used for their isolation.

Compounds $[Zn(tr_2ad)Cl_2]_n$ and $\{[Cu(tr_2ad)Cl]Cl{\cdot}4H_2O\}_n$ were isolated by carrying out a solvothermal reaction among zinc(II) chloride dihydrate and anhydrous copper(II) chloride, respectively, and tr_2ad in the 2:1 molar ratio (DMF, 150 °C, 24 h). Also, the formation of compounds $[Cd_2(tr_2ad)Cl_4]_n$, $\{[Cu(tr_2ad)(NO_3)](NO_3)\}_n$ and $\{[Cd(tr_2ad)(NO_3)](NO_3){\cdot}H_2O\}_n$ required the application of solvothermal conditions, reacting anhydrous cadmium(II) chloride, copper(II) nitrate hemipentahydrate and cadmium(II) nitrate tetrahydrate, respectively, with tr_2ad in the 1:1 molar ratio (methanol, 100 °C, 24 h). All the compounds were isolated, in reasonable yields (55–70%), in the form of air- and moisture-stable microcrystalline powders, insoluble in water and in most common organic solvents (see Section 3.2).

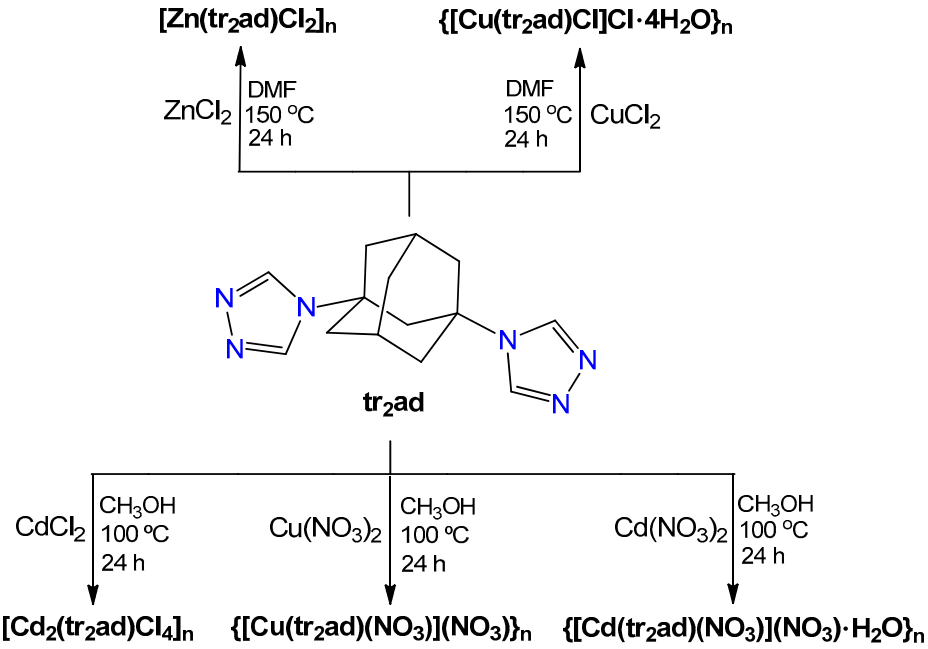

Scheme 2. Synthetic paths for the formation of the tr_2ad-based coordination polymers (CPs) described in this work.

The IR spectrum of the tr_2ad ligand (Figure S1, Supplementary Materials) shows a strong absorption band at 1517 cm^{-1}, which is assigned to the stretching vibration of the triazolyl ring [36]. In the case of the title CPs, this absorption is shifted towards higher wavenumbers (1551–1539 cm^{-1}), as a consequence of the ligand coordination to the metal ions (Figure 1). The medium-intensity broad bands centered around 3400 cm^{-1} in the IR spectra of compounds $\{[Cu(tr_2ad)Cl]Cl{\cdot}4H_2O\}_n$ and $\{[Cd(tr_2ad)(NO_3)](NO_3){\cdot}H_2O\}_n$ (Figure 1), characteristic of the O–H stretching vibration, witness the presence of water molecules.

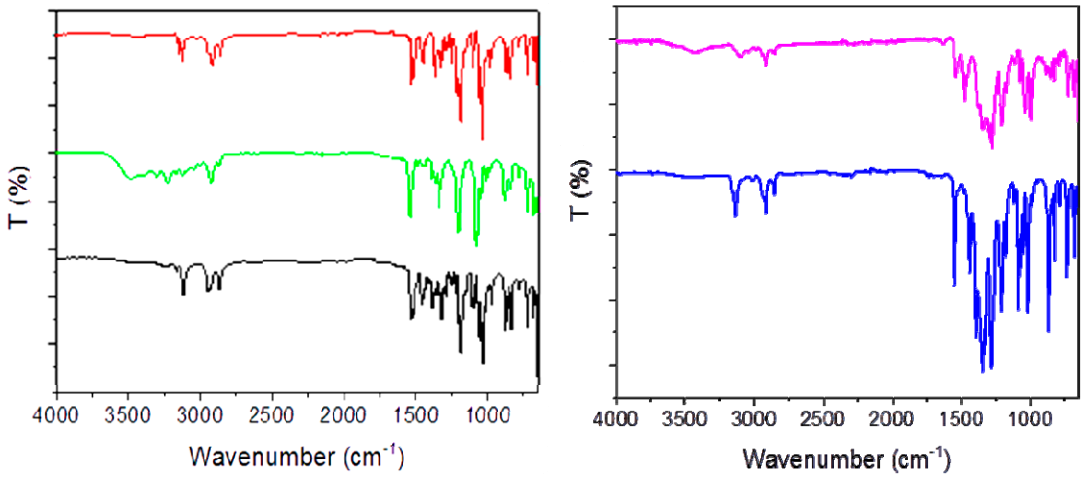

Figure 1. IR spectra of $[Zn(tr_2ad)Cl_2]_n$ (black), $\{[Cu(tr_2ad)Cl]Cl{\cdot}4H_2O\}_n$ (green), $[Cd_2(tr_2ad)Cl_4]_n$ (red), $\{[Cu(tr_2ad)(NO_3)](NO_3)\}_n$ (blue) and $\{[Cd(tr_2ad)(NO_3)](NO_3){\cdot}H_2O\}_n$ (fuchsia).

A deeper analysis of the IR spectra of $\{[Cu(tr_2ad)(NO_3)](NO_3)\}_n$ and $\{[Cd(tr_2ad)(NO_3)](NO_3){\cdot}H_2O\}_n$ (Figure 1) allows to differentiate among the uncoordinated and coordinated forms of the nitrate anion. Indeed, the strong bands located at 1439 and 1282 cm^{-1} for $\{[Cu(tr_2ad)(NO_3)](NO_3)\}_n$, and at 1478 and 1275 cm^{-1} for $\{[Cd(tr_2ad)(NO_3)](NO_3){\cdot}H_2O\}_n$, assigned to the asymmetric and symmetric stretching vibrations of the nitrate group, together with the presence of two very weak bands, at 1755 and

1733 cm^{-1} for $\{[Cu(tr_2ad)(NO_3)](NO_3)\}_n$ and at 1748 and 1717 cm^{-1} for $\{[Cd(tr_2ad)(NO_3)](NO_3)\cdot H_2O\}_n$, suggest the presence of μ_2:η^2 nitrate anions [37,38]. At variance, the bands observed at 1394 and 1346 cm^{-1} for $\{[Cu(tr_2ad)(NO_3)](NO_3)\}_n$ and at 1374 and 1339 cm^{-1} for $\{[Cd(tr_2ad)(NO_3)](NO_3)\cdot H_2O\}_n$, together with the band centered at 1073 cm^{-1} in $\{[Cu(tr_2ad)(NO_3)](NO_3)\}_n$ and at 1076 cm^{-1} in $\{[Cd(tr_2ad)(NO_3)](NO_3)\cdot H_2O\}_n$, can be ascribed to the asymmetric and symmetric stretching modes of uncoordinated nitrate anions [39].

2.2. Thermal Behaviour

Thermogravimetric analyses (TGAs) were performed on the five compounds from 30 °C to 700 °C under a flow of nitrogen. The resulting TGA curves are gathered in Figure 2. Compound $[Zn(tr_2ad)Cl_2]_n$ is stable up to 350 °C, temperature at which a slow decomposition begins. In the temperature range 30–120 °C, $\{[Cu(tr_2ad)Cl]Cl\cdot 4H_2O\}_n$ undergoes a weight loss of ca. 15%, which reasonably corresponds to the evolution of four water molecules per formula unit (calculated weight loss 15.1%).

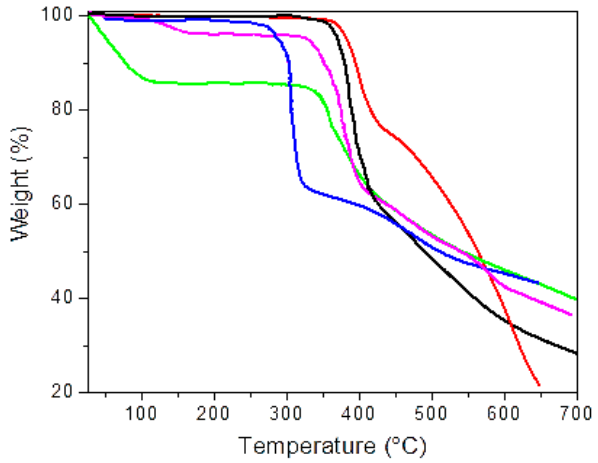

Figure 2. Thermogravimetric analysis (TGA) traces of $[Zn(tr_2ad)Cl_2]_n$ (black), $\{[Cu(tr_2ad)Cl]Cl\cdot 4H_2O\}_n$ (green), $[Cd_2(tr_2ad)Cl_4]_n$ (red), $\{[Cu(tr_2ad)(NO_3)](NO_3)\}_n$ (blue) and $\{[Cd(tr_2ad)(NO_3)](NO_3)\cdot H_2O\}_n$ (fuchsia).

After solvent loss, no further weight loss is observed up to the decomposition onset at 325 °C. Upon heating, compound $\{[Cu(tr_2ad)(NO_3)](NO_3)\}_n$ does not undergo any weight loss up to 250 °C, the temperature at which decomposition starts. To the best of our knowledge, the only known 2-D coordination polymers containing the tr_2ad ligand of which the thermal behavior have been studied are $[Cu^{II}_2(tr_2ad)_4](Mo_8O_{26})$, $[Cu^{II}_4(\mu_4\text{-}O)(tr_2ad)_2(MoO_4)_3]\cdot 7.5H_2O$ [40] and $[Cu_3(tr_2ad)_4(H_2O)_4](SiF_6)_3\cdot 16H_2O$ [41], which decompose at 310 °C, 240 °C and 190 °C, respectively. Compound $[Cd_2(tr_2ad)Cl_4]_n$ displays the highest thermal robustness, peaking up to 365 °C. Until this temperature, no weight loss is observed. Finally, compound $\{[Cd(tr_2ad)(NO_3)](NO_3)\cdot H_2O\}_n$ undergoes a weight loss of ca. 3.5% in the range 30–150 °C, which reasonably corresponds to the release of one water molecule per formula unit (calculated weight loss 3.4%). After this event, no further weight losses are observed up to the decomposition onset at 330 °C. To the best of our knowledge, in no case the thermal behavior of the known Cd^{II} 2-D coordination polymers containing the tr_2ad ligand has been investigated, so that a comparison cannot be carried out. For the title compounds, at the end of the heating process, black residues, possibly containing carbonaceous species, have been recovered.

2.3. Crystal and Molecular Structures

Tr_2ad crystallizes in the monoclinic space group $P2_1/n$. The asymmetric unit contains one tr_2ad molecule in general position. Figure S2a shows the Ortep drawing at 40% probability level. Due to the

lack of conventional hydrogen-bond donors, the crystal structure of tr_2ad only features a network of weak CH···N interactions, with shortest C···N distances of 3.350(2) Å. Both triazole and adamantane CH groups act as unconventional hydrogen bond donors, and most of these non-bonding interactions are directional. Two pairs of such CH···N interactions, together with a slipped π/π interaction among adjacent triazole rings (centroid-centroid distance 3.82 Å, slippage angle 6.6°), concur to the formation of tr_2ad centrosymmetric dimers (Figure 3a). Such self-association is reminiscent of the pairing of 1,3,5-triphenyladamantane molecules prompted by weak CH···π interactions [42].

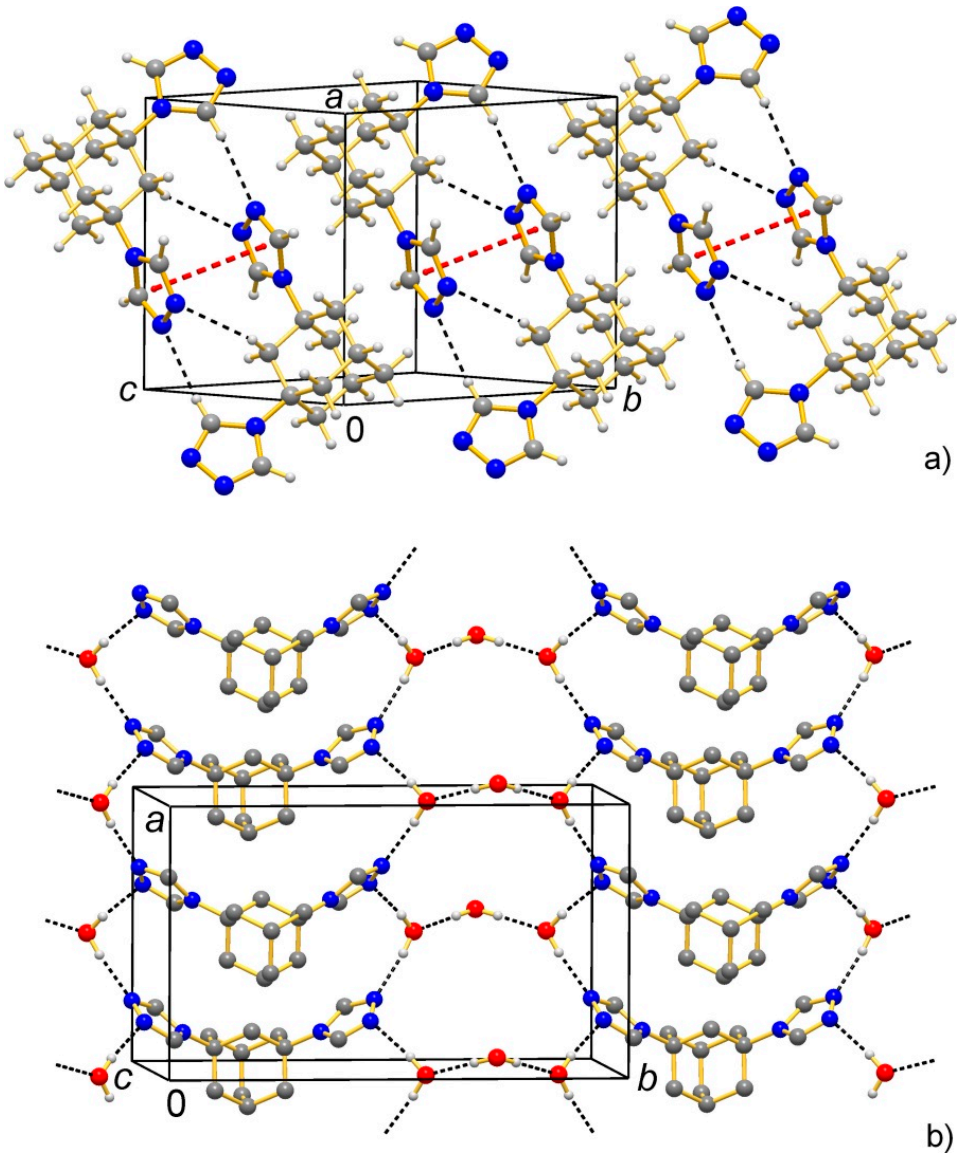

Figure 3. Representation of portion of the crystal structure of (**a**) tr_2ad and (**b**) $tr_2ad{\cdot}3H_2O$, showing the principal supramolecular motifs created by non-bonding interactions involving the triazole nitrogen atoms as acceptors: (**a**) multiple CH···N interactions (black dashed lines) concur with π/π stacking interactions (red dashed lines) to form tr_2ad dimers; (**b**) OH···N and OH···O hydrogen bonds (black dashed lines) support the formation of 2-D supramolecular layers. Atoms colour code: C, grey; H, light grey; N, blue; O, red.

The hydrate ligand $tr_2ad{\cdot}3H_2O$ crystallizes in the orthorhombic space group *Pnma*. The asymmetric unit contains half of a tr_2ad molecule and half of a H_2O molecule, both situated across a mirror plane (Wyckoff letter *c*), and one water molecule in general position. Figure S2b shows the Ortep drawing at 30% probability level. The primary intermolecular interactions in the crystal structure are conventional

OH···N hydrogen bonds (O···N = 2.896(3), 2.932(3) Å) involving all the triazole nitrogen atoms as acceptors. These interactions assemble the tr_2ad and water molecules (in a 1:2 ratio) into 1-D strips along the crystallographic *a*-axis (Figure 3b). Additional water molecules establish bridges between the strips through pairs of symmetry-equivalent OH···O bonds (O···O = 2.764(2) Å) (Figure 3b). The 2-D hydrogen-bond connectivity comprises water trimers H_2O···H–O–H···OH_2 linked to four triazole-N sites. Overall, the crystal structures of tr_2ad and $tr_2ad{\cdot}3H_2O$ reveal the potentiality of triazole-N^1,N^2 atoms as efficient hydrogen-bond acceptors.

Compound $[Zn(tr_2ad)Cl_2]_n$ crystallizes in the orthorhombic space group $P2_12_12_1$. The asymmetric unit contains one Zn^{II} ion, one tr_2ad ligand and two chloride anions, all in general positions. The metal centre shows a $ZnCl_2N_2$ tetrahedral stereochemistry (Figure 4a; the Figure caption collects the values of the bond distances and angles at the metal ion), defined by two chloride anions and the nitrogen atoms of the triazole rings of two tr_2ad ligands. The ligands are exo-bidentate (μ_2-κN^1:$\kappa N^{1'}$) and bridge neighbouring Zn^{II} ions along 1-D polymeric chains (Figure 4b) of pitch 11.120(4) Å parallel to the [001] crystallographic direction (this occurrence rationalizing the preferred orientation pole; see Section 3.3). The chains pack in the *ab* plane defining a rectangular motif (Figure 4c). Non-bonding interactions of the kind C–H···N (C···N 3.2 Å) and C–H···Cl involving both chloride anions (C···Cl 3.5–3.7 Å) are at work within the chains and between nearby chains, respectively. No empty volume is present [43].

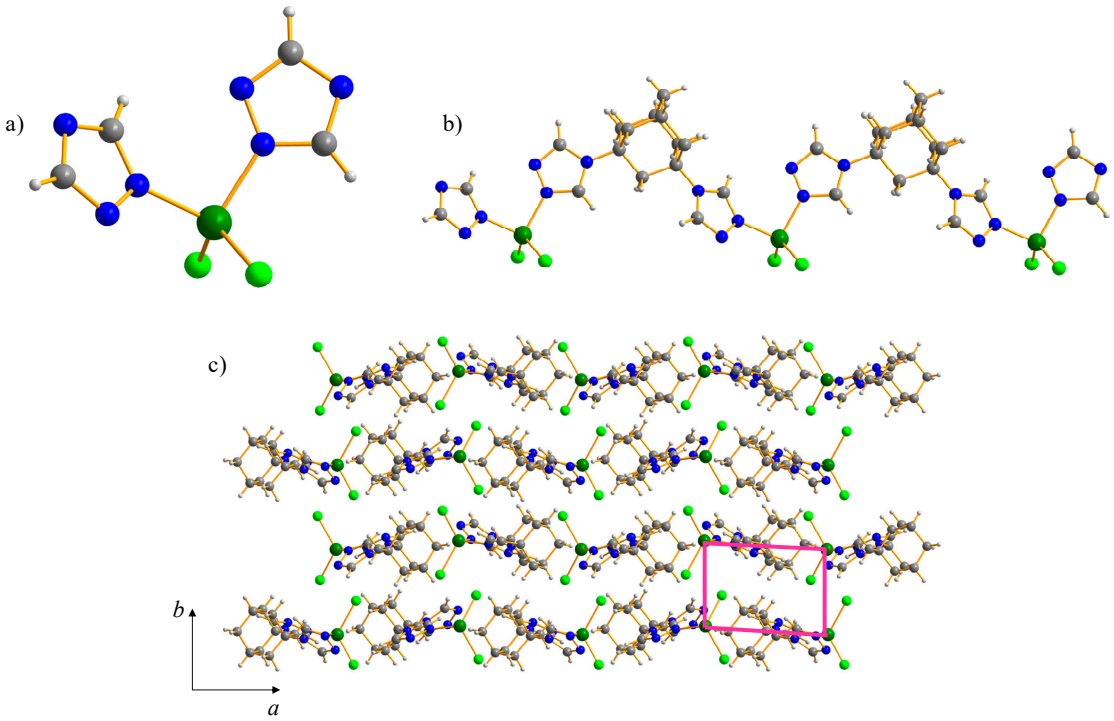

Figure 4. Representation of the crystal structure of $[Zn(tr_2ad)Cl_2]_n$: (**a**) the coordination sphere of the Zn^{II} ions; (**b**) portion of the 1-D polymeric motif running along the [001] crystallographic direction; (**c**) portion of the packing, viewed along the [001] crystallographic direction. Horizontal axis, *a*; Vertical axis, *b*. Highlighted in fuchsia the rectangular packing of the 1-D chains. Atoms colour code: C, grey; H, light grey; Cl, light green; N, blue; Zn, green. Main bond distances (Å) and angles (°) at the metal ions: Zn–Cl 2.153(7), 2.316(7); Zn–N 1.944(9), 2.01(1); shortest intra-chain Zn···Zn 11.120(3); N–Zn–N 99.5(5); Cl–Zn–Cl 117.7(2); Cl–Zn–N 107.0(6), 107.1(5), 110.0(5), 113.7(7).

Compound $\{[Cu(tr_2ad)Cl]Cl{\cdot}4H_2O\}_n$ crystallizes in the monoclinic space group $P2_1/m$. The asymmetric unit is composed by half of a metal centre (on an inversion centre, Wyckoff letter *b*), half of a tr_2ad ligand, two halves of a chloride anion and two halves of a water molecule (all on mirror planes, Wyckoff letter *e*), as well as one water molecule (in general position). The Cu^{II} ions are hexa-coordinated in *trans*-$CuCl_2N_4$ octahedral geometry defined by the nitrogen atoms of four tr_2ad ligands and one

of the two independent chloride anions (Figure 5a; the main bond distances and angles at the metal ions are reported in the Figure caption). μ-coordination by triazole rings and coordinated chloride anions brings about the formation of 1-D helices of metal ions (Figure 5b) with pitch 3.5863(2) Å (half of the *b*-axis) running along the crystallographic direction [010]. The tr_2ad ligands, which are overall exo-tetradentate (μ_4-κN^1:κN^2:$\kappa N^{1'}$:$\kappa N^{2'}$), connect the helices along the crystallographic direction [001], bringing about the formation of 2-D double-layers parallel to the *bc* crystallographic plane (Figure 5c). The layers pack, staggered, along the *a*-axis. The second independent chloride anion and one of the four independent water molecules occupy the rhombic cavities formed by the ligands within the double-layers (Figure 5c) and are involved in a HO–H···Cl non-bonding interaction (O···Cl 2.58(3) Å; Figure S7a). The other three water molecules are located in the inter-layer space and, by means of hydrogen bonds (O···O 2.44(2), 2.91(2), 3.07(2) Å; Figure S3a), define a 1-D supramolecular chain running parallel to the *b*-axis. Finally, the double layers are reinforced by C–H···Cl interactions (C···Cl 3.3–3.4 Å; Figure S3b). No empty volume is envisaged [43].

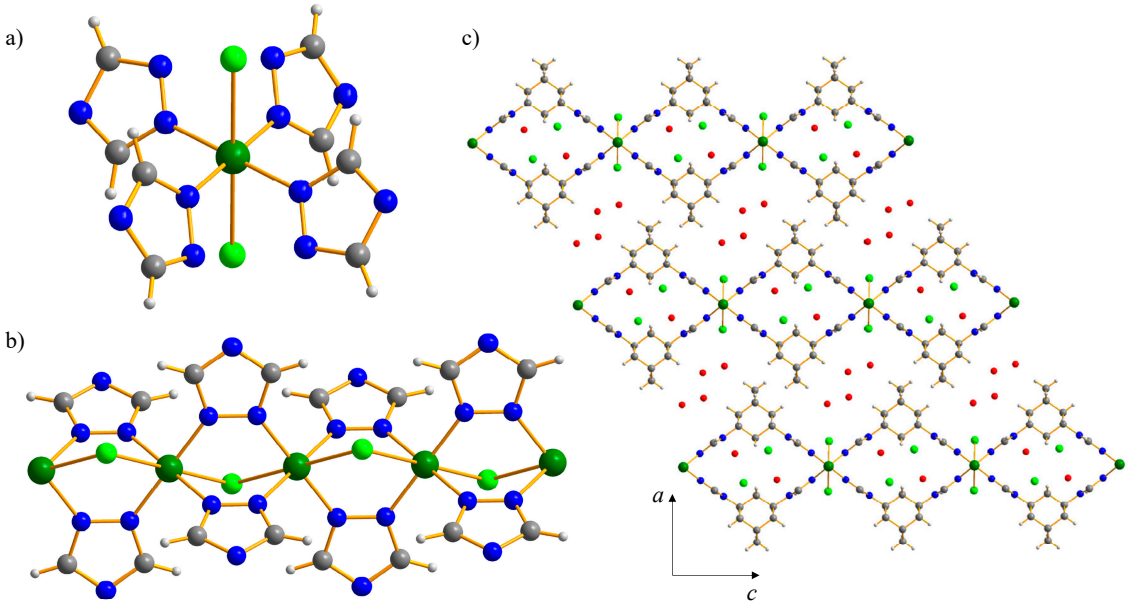

Figure 5. Representation of the crystal structure of $\{[Cu(tr_2ad)Cl]Cl{\cdot}4H_2O\}_n$: (**a**) the coordination sphere of the metal ions; (**b**) portion of the 1-D helix; (**c**) portion of the packing, viewed along the [010] crystallographic direction. Horizontal axis, *c*; vertical axis, *a*. For the non-bonding interactions quoted in the text the reader is addressed to Figure S3. Atoms colour code: C, grey; H, light grey; Cl, light green; Cu, green; N, blue; O, red. Main bond distances (Å) and angles (°) at the metal ions: Cu–Cl 2.632(7); Cu–N 1.969(4), 2.009(6); shortest Cu···Cu intra-chain 3.5863(2); shortest Cu···Cu inter-chain 10.9798(7); N–Cu–N 80.4(3), 99.6(3), 180; Cl–Cu–Cl 180; Cl–Cu–N 88.1(3), 89.7(3), 90.3(3), 91.9(3).

Compound $[Cd_2(tr_2ad)Cl_4]_n$ crystallizes in the triclinic space group *P*-1. The asymmetric unit equals the formula unit, i.e., it contains two cadmium(II) ions, four chloride anions and one tr_2ad ligand, all in general positions. Both independent metal centres are hexa-coordinated and show an octahedral stereochemistry, though of different kind, namely: *cis*-CdN_2Cl_4 and $CdNCl_5$ (Figure 6a; the main bond distances and angles at the metal ions are reported in the Figure caption). Three of the four chloride anions bridge adjacent metal centres, while the fourth one behaves as a terminal ligand. The tr_2ad spacer is exo-tridentate (μ_3-κN^1:κN^2:$\kappa N^{1'}$). The reciprocal disposition of cations and anions brings about the formation of 1-D polymeric strands (Figure 6b) running along the [100] crystallographic direction. The tr_2ad linkers bridge nearby strands leading to the formation of 2-D double-layers parallel to the (01-1) plane and packing, staggered, along the [011] direction (Figure 6c). The reciprocal disposition of the spacers within a layer brings about the formation of intra-layer rhombic cavities, in which the terminal chloride anions are directed (Figure 6c). This structural motif is

analogous to that found in $\{[Cu(tr_2ad)Cl]Cl{\cdot}4H_2O\}_n$ (see above). Weak intra- and inter-layer C–H···Cl interactions (C···Cl 3.3–3.7 Å) are present. No empty volume is observed [43].

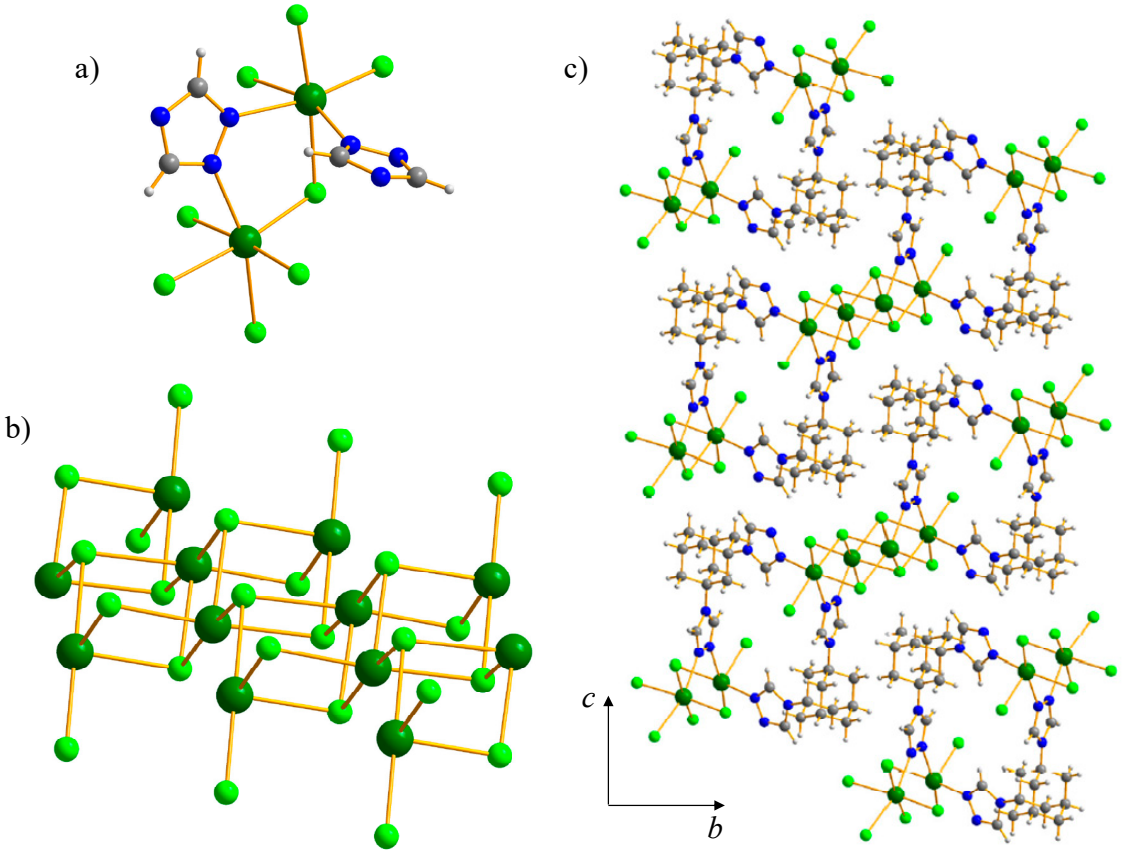

Figure 6. Representation of the crystal structure of $[Cd_2(tr_2ad)Cl_4]_n$: (**a**) the coordination sphere of the metal ions; (**b**) portion of the 1-D polymeric strands; (**c**) portion of the packing, viewed along the [100] crystallographic direction. Horizontal axis, *b*; vertical axis, *c*. Atoms colour code: C, grey; H, light grey; Cl, light green; Cd, green; N, blue. Main bond distances (Å) and angles (°) at the metal ions: Cd1–Cl 2.59(2), 2.62(2), 2.75(2), 2.82(2), 2.87(2); Cd1–N 2.42(3); Cd2–Cl 2.58(2), 2.59(1), 2.62(2), 2.78(2); Cd2–N 2.32(2), 2.32(3); shortest intra-strand Cd···Cd 3.842(8)–4.241(8); shortest inter-strand Cd···Cd 7.526(7) Cl–Cd1–N 84(1)–165.0(1); Cl–Cd1–Cl 82.5(5)–174.2(5); Cl–Cd2–N 77(1)–165(1); Cl–Cd2–Cl 85.6(5)–173.5(6); N–Cd2–N 92.2(8).

Compound $\{[Cu(tr_2ad)(NO_3)](NO_3)\}_n$ crystallizes in the orthorhombic space group *Pnma*. The asymmetric unit is composed by one Cu^{II} ion, two halves of nitrate anions and half of a tr_2ad spacer, all lying on mirror planes (Wyckoff letter *h*). The metal centre is hexa-coordinated in *trans*-CuN_4O_2 stereochemistry (Figure 7a; the main bond distances and angles at the metal ions are reported in the Figure caption), defined by four tr_2ad linkers and one of the two independent nitrate anions. The latter bridges (μ_2-κO^1:κO^2) nearby metal centres 3.54(2) Å apart, while the other nitrate anion is not coordinated. The tr_2ad ligand is exo-tetradentate (μ_4-κN^1:κN^2:$\kappa N^{1'}$:$\kappa N^{2'}$). μ_2-bridging of the nitrate anions and triazole rings brings about the formation of 1-D chains running along the [100] direction (Figure 7b).

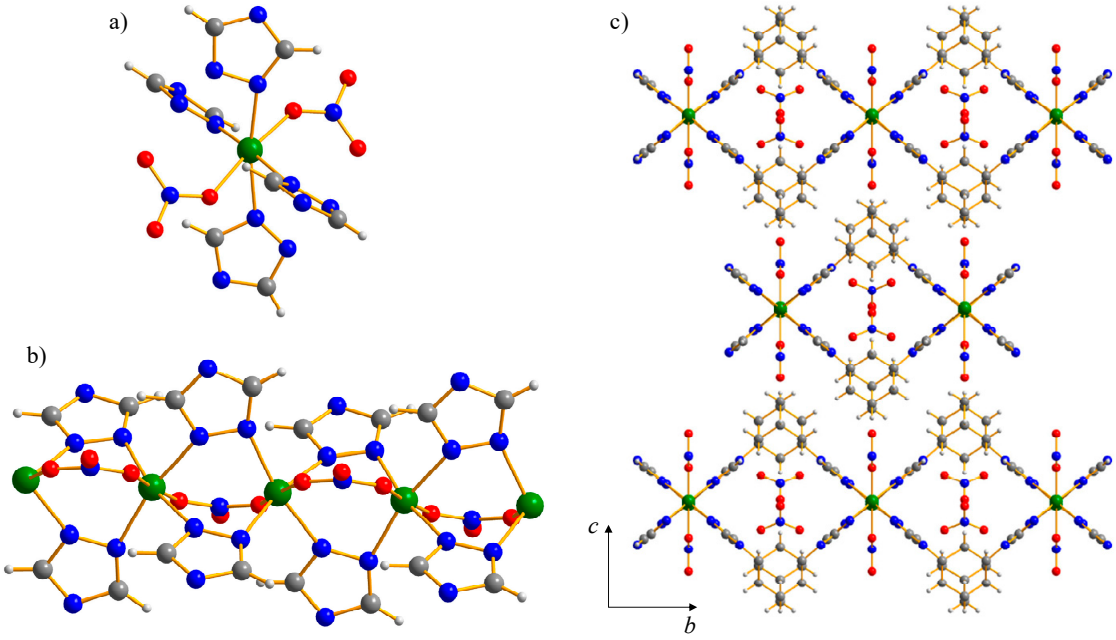

Figure 7. Representation of the crystal structure of $\{[Cu(tr_2ad)(NO_3)](NO_3)\}_n$: (**a**) the coordination sphere of the metal ions; (**b**) portion of the 1-D polymeric chain; (**c**) portion of the packing, viewed along the [100] crystallographic direction. Horizontal axis, *b*; vertical axis, *c*. Atoms colour code: C, grey; H, light grey; Cu, green; N, blue; O, red. Main bond distances (Å) and angles (°) at the metal ions: Cu–N 2.03(1), 2.148(9); Cu–O 2.09(2), 2.26(2); intra-chain shortest Cu···Cu 3.54(2); inter-chain shortest Cu···Cu 10.7226(7); N–Cu–N 76.4(6), 97.01(3), 173.5(5); O–Cu–O 180(1); O–Cu–N 68.9(5), 70.3(6), 109.8(6), 111.0(6).

Nearby chains are connected along [010] by the tr_2ad spacers within 2-D polymeric double-layers parallel to the (001) plane and packing, staggered, along the [001] direction (Figure 7c; this occurrence explains the preferred orientation pole—see Section 3.3). The reciprocal disposition of the tr_2ad linkers within a layer brings about the formation of intra-layer rhombic cavities, in which the not coordinated nitrate anions are located (Figure 7c) and involved in C–H···O non-bonding interactions (C···O 2.6–3.2 Å). The structural motif is analogous to that found in the Cu^{II} and Cd^{II} compounds described above. No empty volume is observed [43].

Compound $\{[Cd(tr_2ad)(NO_3)](NO_3)\cdot H_2O\}_n$ crystallizes in the monoclinic space group *C*2/*c*. The asymmetric unit contains two halves of Cd^{II} ions (one on an inversion centre, Wyckoff position *b*, the other one on a two-fold axis, Wyckoff position *e*), two nitrate anions, one tr_2ad ligand and one water molecule—all in general positions. The metal centres are hexa-coordinated in *trans*-CdN_4O_2 octahedral stereochemistry defined by four ligands and two nitrate anions (Figure 8a; the main bond distances and angles at the metal ions are reported in the Figure caption). One of the two independent nitrate anions bridge (μ_2-κO^1:κO^2) neighbouring metal centres, while the other one is not coordinated. The tr_2ad spacer is exo-tetradentate (μ_4-κN^1:κN^2:$\kappa N^{1'}$:$\kappa N^{2'}$). μ_2-Coordination of the nitrate anions and triazole rings is responsible for the formation of 1-D chains parallel to the [001] crystallographic direction (Figure 8b). Adjacent chains are bridged along the [010] direction to yield 2-D double-layers parallel to the *bc* plane and packing, staggered, along the *a*-axis (Figure 8c; this occurrence explains the preferred orientation pole—see Section 3.3). The reciprocal disposition of the tr_2ad linkers within a layer brings about the formation of intra-layer rhombic cavities, in which the not coordinated nitrate anions are located (Figure 8c). The structural motif is analogous to that found in the Cu^{II} and Cd^{II} compounds described above. The water molecules are located in the inter-layer space (Figure 8c) and are involved in C–H···O non-bonding interactions (C···O 2.9–3.2 Å) with adjacent tr_2ad ligands. No empty volume is observed [43].

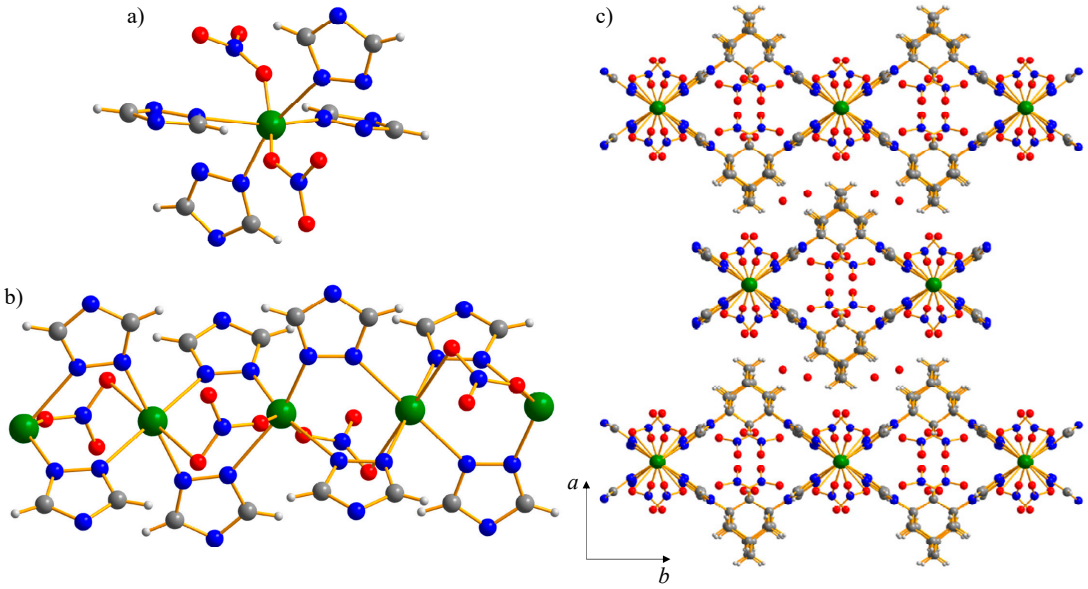

Figure 8. Representation of the crystal structure of $\{[Cd(tr_2ad)(NO_3)](NO_3)\cdot H_2O\}_n$: (**a**) the coordination sphere of the metal ions; (**b**) portion of the 1-D polymeric chains; (**c**) portion of the packing, viewed in perspective along the [001] crystallographic direction. Horizontal axis, *b*; vertical axis, *a*. Atoms colour code: C, grey; H, light grey; Cu, green; N, blue; O, red. Main bond distances (Å) and angles (°) at the metal ions: Cd1–N 2.24(1), 2.30(1); Cd1–O 1.54(3); Cd2–N 2.17(1), 2.23(1); Cd2–O 2.79(4); intra-chain Cd···Cd 3.8724(3); inter-chain Cd···Cd 11.39(2); N–Cd1–N 80.2(5)–176.3(5); O–Cd1–O 168(3); N–Cd1–O 72(1)–105(1); N–Cd2–N 88.7(6), 91.3(6), 180; O–Cd2–O 180; N–Cd2–O 68(1)–110.1(8).

2.4. Comparative Structure Analysis

A search in the Cambridge Structural Database (v 2020.1) for coordination compounds containing the tr_2ad ligand has revealed the existence of 22 coordination polymers. Table 1 collects key structural aspects (coordination sphere and geometry at the metal ion, tr_2ad ligand hapticity, polymer dimensionality) of these compounds. The following observations can be carried out:

1. Among the CPs retrieved in the literature (Table 1), 14 contain Cu^{II} or Cd^{II}, while the others feature Cu^{I}, Ag^{I}, Mo^{II} or Fe^{II}. Hence, to the best of our knowledge, $[Zn(tr_2ad)Cl_2]_n$ is the first example of Zn^{II}-based coordination compound containing the tr_2ad ligand.
2. As regards the stereochemistry at the metal ion, apart from $[Cd_3(tr_2ad)_2I_6]$, in which one of the two independent Cd^{II} ions shows a tetrahedral geometry, in all the known Cd^{II} CPs the metal centre adopts an octahedral geometry, as in $[Cd(tr_2ad)Cl_4]_n$ and $\{[Cd(tr_2ad)(NO_3)](NO_3)\cdot H_2O\}_n$. On the other hand, while in $\{[Cu(tr_2ad)Cl]Cl\cdot 4H_2O\}_n$ and $\{[Cu(tr_2ad)(NO_3)](NO_3)\}_n$ the metal ion is in octahedral stereochemistry, in the known CPs the Cu^{II} coordination number varies in the range 4–6, with different coordination geometries associated (Table 1).
3. Upon comparing the values of the M–N distances (M = Cu^{II} or Cd^{II}, N = tr_2ad nitrogen atom), it appears (Figure S4) that the novel materials share distances comparable with those of the literature CPs.
4. Apart from $[Zn(tr_2ad)Cl_2]_n$, all the other compounds studied in this work are 2-D coordination polymers characterized by the same structural motif (see Figures 4–8). At variance, Table 1 shows that in the known compounds the dimensionality ranges from 1-D to 3-D. Interestingly, the structural motif observed in the title Cu^{II} and Cd^{II} derivatives, with rhombic cavities within 2-D strands, is shown also by COVFIE, COVFOK, KEHDEI, KEMLEV and TUGSIY, containing Cu^{II} or Cd^{II} ions, and UZAKIQ, containing the Mo^{II} ion.

Table 1. Main structural properties of the known coordination polymers containing the tr_2ad ligand. Abbreviations: M = metal ion; OC = octahedral; SP = square planar; SQP = square pyramidal; TB = trigonal bipyramidal; TD = tetrahedral; TP = trigonal planar; H_3btc = 1,3,5-benzenetricarboxylic acid; H_4adtc = 1,3,5,7-adamantane-tetracarboxylic acid; [a] M–F.

CSD Code	Molecular Formula	M Stereochemistry	M Geometry	M–N (Å)	M–X (Å)	Tr_2ad Apticity	Dim.	Ref.
COVFIE	$[Cu_2(tr_2ad)_4](Mo_8O_{26})$	CuN_5	SP	1.968–2.247	-	Exo-bidentate Exo-tridentate	2-D	[40]
COVFOK	$[Cu_4(tr_2ad)_2(\mu_4\text{-}O)(MoO_4)_3]\cdot 7.5H_2O$	CuN_2O_3 CuN_2O_3 CuN_2O_3	TB TB TB	2.078, 2.093 2.005 2.009	1.923–2.028 1.937–2.090 1.937–2.067	Exo-tetradentate (2×)	2-D	[40]
COVFUQ	$[Cu_2(tr_2ad)_2](Mo_2O_7)\cdot H_2O$	CuN_3 CuN_3	TP TP	1.928–2.002 1.934–2.000	- -	Exo-tridentate (2×)	1-D	[40]
KEMLEV	$[Cu(tr_2ad)(SO_4)]\cdot 3H_2O$	*trans*-CuN_4O_2	OC	2.009–2.012	2.406	Exo-tetradentate	2-D	[41]
KEMLIZ	$[Cu_3(tr_2ad)_4(H_2O)_2(SO_4)_2](SO_4)\cdot 28H_2O$	CuN_6 CuN_4O	OC SQP	2.024–2.365 1.995–2.223	- 1.958	Exo-tetradentate Exo-tridentate	2-D	[41]
KEMLOF	$[Cu_3(tr_2ad)_4(H_2O)_2](SiF_6)_3\cdot 16H_2O$	CuN_6 *cis*-CuN_4O_2	OC OC	2.001-2.413 1.988–2.269	- 1.987, 2.554	Exo-tetradentate Exo-tridentate	2-D	[41]
PODMAX	$[Cu_4(tr_2ad)_2(btc)_2(\mu_3\text{-}OH)_2]$	$CuNO_4$ CuN_2O_3	SQP TB	2.411 1.989–2.010	1.915–1.999 1.953–2.165	Exo-tridentate	3-D	[44]
SERCUP	$[Cu_4(tr_2ad)_2(H\text{-}adtc)_2(OH)_2(H_2O)_2]\cdot 4H_2O$	$CuNO_5$ *cis*-CuN_2O_4 CuN_2O_3 $CuNO_4$	OC OC SQP SQP	1.981 1.989–2.334 2.005–2.271 1.987	1.905–2.685 1.957–2.691 1.950–1.996 1.923–2.279	Exo-tridentate	2-D	[45]
TUGSUK	$[Cu_3(tr_2ad)_4(SO_4)(H_2O)_3](SO_4)_2\cdot 34H_2O$	CuN_6 *cis*-CuN_4O_2 CuN_4O	OC OC SQP	1.989–2.295 1.990–2.250 1.957–2.291	- 1.989, 2.408 1.989	Exo-tetradentate (2×) Exo-tridentate (2×)	3-D	[46]
TUGTAR	$[Cu_2(\mu\text{-}OH)(tr_2ad)_2](NO_3)_3\cdot 4H_2O$	CuN_6 *cis*-CuN_4O_2 *trans*-CuN_2O_4	OC OC OC	2.026–2.527 1.982–2.212 2.000	- 1.921–2.788 1.909–2.686	Exo-tetradentate (2×)	3-D	[46]
ILUFEB	$[Cd_3(tr_2ad)_3](SeCN)_6$	CdN_6 CdN_6	OC OC	2.289–2.370 2.332–2.353	- -	Exo-tridentate (4×)	3-D	[47]
KEHDEI	$[Cd_2(tr_2ad)_2(H_2O)_4](CdBr_4)_2$	*cis*-CdN_4O_2 *cis*-CdN_4O_2 $CdBr_4$	OC OC TD	2.266–2.343 2.273–2.323 -	2.377–2.382 2.370–2.406 2.567–2.629	Exo-bidentate (4×)	3-D	[48]

Table 1. *Cont.*

CSD Code	Molecular Formula	M Stereochemistry	M Geometry	M–N (Å)	M–X (Å)	Tr_2ad Apticity	Dim.	Ref.
KEHDIM	$[Cd_3(tr_2ad)_2I_6]$	CdN_6 $CdNI_3$	OC TD	2.305–2.403 2.283	- 2.744–2.756	Exo-bidentate (2×)	2-D	[48]
TUGSIY	$[Cd_3(tr_2ad)_3(\mu\text{-}NCS)_3](NCS)_3$	$CdN_{1-x}S_x$ ($0 < x < 1$) CdN_6	OC OC	2.296–2.473 2.312–2.405	2.662	Exo-tetradentate (3×)	2-D	[46]
TUGSOE	$[Cd_3(tr_2ad)_6](NO_3)_6{\cdot}22H_2O$	CdN_6 CdN_6	OC OC	2.324–2.356 2.297–2.381	-	Exo-tridentate (3×)	3-D	[46]
HUSQES	$[Mo_2(tr_2ad)O_6]{\cdot}6H_2O$	*cis*-MoN_2O_4	OC	2.366, 2.375	1.702–1.932	Exo-tetradentate	3-D	[49]
LUYRII	$[Mo_2(tr_2ad)O_6]{\cdot}H_2O$	*cis*-MoN_2O_4	OC	2.405	1.714–1.910	Exo-tetradentate	2-D	[50]
UZAKIQ	$[Mo_2(tr_2ad)F_2O_5]$	MoN_2O_3F MoN_2O_3F	OC OC	2.399 2.380	1.710–1.918 1.917 [a] 1.706–1.914 1.934 [a]	Exo-tetradentate	1-D/2-D	[51]
VEPDEB	$\{Fe_3(tr_2ad)_4[Au(CN)_2]_2\}[Au(CN)_2]_4{\cdot}8H_2O$	FeN_6 FeN_6	OC OC	1.910–1.970 1.975–1.987	- -	Exo-tetradentate (2×) Exo-tridentate	3-D	[52]
KEHDOS	$[Ag(tr_2ad)](NO_3){\cdot}H_2O$	AgN_4 AgN_4	TD TD	2.185–2.502 2.185–2.528	- -	Exo-tetradentate (2×)	3-D	[48]
WEJWAL	$[Ag(tr_2ad)](ClO_4)$	AgN_3	TP	2.191–2.347	-	Exo-tridentate	2-D	[53]
WEJWEP	$[Ag_2(tr_2ad)_2(VO_2F_2)_2]{\cdot}H_2O$	AgN_3O	TD	2.209–2.464	2.558	Exo-tetradentate	1-D	[53]

3. Materials and Methods

3.1. General

All reagents and solvents were purchased from Sigma-Aldrich (Darmstadt, Germany) and used as received, without further purification. The ligand 1,3-bis(1,2,4-triazol-4-yl)adamantane (tr_2ad) was synthesized by the acid-catalyzed condensation reaction of 1,3-diaminoadamantane and *N*,*N*-dimethylformamide azine, according to an already reported method [46]. A detailed description regarding the preparation of the intermediates (Scheme S1), on which no details have ever been reported before, is provided in the Supplementary Materials. NMR spectra (DMSO-d_6, δ, ppm) were recorded on a Bruker 400 MHz spectrometer. The IR spectra were recorded from 4000 to 650 cm^{-1} with a PerkinElmer Spectrum 100 instrument (Perkin-Elmer, Shelton, CT, USA) by attenuated total reflectance on a CdSe crystal. Elemental analyses (carbon, hydrogen, and nitrogen %) were performed with a Fisons Instruments 1108 CHNS-O elemental analyzer (Thermo Scientific, Waltham, MA, USA). Before the analytical characterization was carried out, all the samples were dried under vacuum (50 °C, ~0.1 Torr) until a constant weight was reached. Thermogravimetric analyses (TGAs) were carried out under a N_2 flow (25 mL/min), in the temperature range 30–700 °C and with a heating rate of 5 °C/min, using a PerkinElmer STA 6000 simultaneous thermal analyzer (Perkin-Elmer, Shelton, CT, USA).

3.2. Synthesis of the Tr_2ad-Based CPs

3.2.1. Synthesis of $[Zn(tr_2ad)Cl_2]_n$

Tr_2ad (0.054 g, 0.2 mmol) was dissolved in *N*,*N*-dimethylformamide (DMF) (5 mL) and the obtained solution was left under stirring at room temperature for 5 min. Then, $ZnCl_2{\cdot}2H_2O$ (0.017 g, 0.1 mmol) was added, and the resulting solution was introduced into a high-pressure glass tube and heated at 150 °C for 24 h. Slow cooling of the solution to room temperature, followed by partial slow evaporation of the solvent, afforded a white solid which was filtered off, washed twice with DMF, dried under vacuum and identified as $[Zn(tr_2ad)Cl_2]$. Yield: 55%. $[Zn(tr_2ad)Cl_2]$ is insoluble in alcohols, acetone, acetonitrile, chlorinated solvents, DMF, dimethylsulfoxide (DMSO) and water. Elem. anal. calc. for $C_{14}H_{18}Cl_2N_6Zn$ (FW = 406.65 g/mol): C, 41.35; H, 4.46; N, 20.67%. Found: C, 40.95; H, 4.23; N, 20.35%. IR (cm^{-1}): 3160(w), 3110(m) ν(C–$H_{aromatic}$), 2930(m), 2870(m) ν(C–$H_{aliphatic}$), 1539(s) ν(C=N), 1387(m), 1329(m), 1192(vs), 1110(m), 1029(vs), 973(w), 883(m), 934(m), 786(w), 728(m), 680(m), 656(vs).

3.2.2. Synthesis of $\{[Cu(tr_2ad)Cl]Cl{\cdot}4H_2O\}_n$

Tr_2ad (0.054 g, 0.2 mmol) was dissolved in DMF (5 mL) and the obtained solution was left under stirring at room temperature for 5 min. Then, $CuCl_2$ (0.013 g, 0.1 mmol) was added, and the resulting solution was introduced into a high-pressure glass tube and heated at 150 °C for 24 h. Slow cooling of the solution to room temperature, followed by slow partial evaporation of the solvent, afforded a light blue solid which was filtered off, washed twice with DMF, dried under vacuum and identified as $[Cu(tr_2ad)Cl]Cl{\cdot}4H_2O$. Yield: 65%. $[Cu(tr_2ad)Cl]Cl{\cdot}4H_2O$ is insoluble in alcohols, acetone, acetonitrile, chlorinated solvents, DMF, DMSO and water. Elem. anal. calc. for $C_{14}H_{26}Cl_2CuN_6O_4$ (FW = 476.91 g/mol): C, 35.26; H, 5.49; N, 17.62%. Found: C, 34.85; H, 5.33; N, 17.25%. IR (cm^{-1}): 3500–3200(br) ν(H–O), 3200–3000(w) ν(C–$H_{aromatic}$), 2921(m), 2864(w) ν(C–$H_{aliphatic}$), 1543(s) ν(C=N), 1346(s), 1207(vs), 1086(vs), 1045(w), 1021(w), 883(m), 842(w), 786(w), 728(m), 680(m).

3.2.3. Synthesis of $[Cd_2(tr_2ad)Cl_4]_n$

Tr_2ad (0.054 g, 0.2 mmol) was dissolved in methanol (5 mL) and the obtained solution was left under stirring at room temperature for 5 min. Then, $CdCl_2$ (0.036 g, 0.2 mmol) was added, and the resulting solution was introduced into a high-pressure glass tube and heated at 100 °C for 24 h. The white precipitate which was formed was filtered off, washed three times with hot methanol, dried under vacuum and identified as $[Cd_2(tr_2ad)Cl_4]$. Yield: 65%. $[Cd_2(tr_2ad)Cl_4]$ is insoluble in

alcohols, acetone, acetonitrile, chlorinated solvents, DMF, DMSO and water. Elem. anal. calc. for $C_{14}H_{18}Cd_2Cl_4N_6$ (FW = 637.00 g/mol): C, 26.40; H, 2.85; N, 13.19%. Found: C, 26.33; H, 2.92; N, 12.85%. IR (cm^{-1}): 3143(w), 3121(m) ν(C–$H_{aromatic}$), 2915(m), 2858(w) ν(C–$H_{aliphatic}$), 1737(m), 1534(m) ν(C=N), 1371(m), 1253(m), 1191(vs), 1105(m), 1069(s), 1046(vs), 990(m), 883(m), 866(m), 850(m), 791(w), 730(m), 681(m), 658(m).

3.2.4. Synthesis of $\{[Cu(tr_2ad)(NO_3)](NO_3)\}_n$

Tr_2ad (0.054 g, 0.2 mmol) was dissolved in methanol (5 mL) and the obtained solution was left under stirring at room temperature for 5 min. Then, $Cu(NO_3)_2{\cdot}2.5H_2O$ (0.037 g, 0.2 mmol) was added, and the resulting solution was introduced into a high-pressure glass tube and heated at 100 °C for 24 h. A green precipitate was formed, which was filtered off, washed three times with hot methanol, dried under vacuum and identified as $[Cu(tr_2ad)(NO_3)](NO_3)$. Yield: 70%. $[Cu(tr_2ad)(NO_3)](NO_3)$ is insoluble in alcohols, acetone, acetonitrile, chlorinated solvents, DMF, DMSO and water. Elem. Anal. calc. for $C_{14}H_{18}CuN_8O_6$ (FW = 457.95 g/mol): C, 36.72; H, 3.96; N, 24.47%. Found: C, 36.35; H, 3.73; N, 24.19%. IR (cm^{-1}): 3136(m), 3016(vw) ν(C–$H_{aromatic}$), 2916(m), 2856(w) ν(C–$H_{aliphatic}$), 1755(vw), 1733(vw), 1551(s) ν(C=N), 1439(s) ν_{asym}(coordinated NO_3), 1394(vs) ν_{asym}(uncoordinated NO_3), 1346(vs) ν_{sym}(uncoordinated NO_3), 1329(vs), 1282(vs) ν_{sym}(coordinated NO_3), 1210(s), 1180(m), 1119(w), 1089(s), 1073(m), 1054(m), 1019(s), 867(vs), 826(m), 787(w), 738(m), 716(w), 681(m).

3.2.5. Synthesis of $\{[Cd(tr_2ad)(NO_3)](NO_3){\cdot}H_2O\}_n$

Tr_2ad (0.054 g, 0.2 mmol) was dissolved in methanol (5 mL) and the obtained solution was left under stirring at room temperature for 5 min. Then, $Cd(NO_3)_2{\cdot}4H_2O$ (0.047 g, 0.2 mmol) was added, and the resulting solution was introduced into a high pressure glass tube and heated at 100 °C for 24 h. The white precipitate which was formed was filtered off, washed three times with hot methanol, dried under vacuum and identified as $[Cd(tr_2ad)(NO_3)](NO_3){\cdot}H_2O$. Yield: 60%. $[Cd(tr_2ad)(NO_3)](NO_3){\cdot}H_2O$ is insoluble in alcohols, acetone, acetonitrile, chlorinated solvents, DMF, DMSO and water. Elem. Anal. calc. for $C_{14}H_{20}CdN_8O_7$ (FW = 524.83 g/mol): C, 32.04; H, 3.84; N, 21.35%. Found: C, 31.87; H, 3.55; N, 20.98%. IR (cm^{-1}): 3418(br) ν(H–O), 3098(w), 3043(w) ν(C–$H_{aromatic}$), 2916(m), 2869(w), 2853(w) ν(C–$H_{aliphatic}$), 1748(vw), 1717(vw), 1633(w), 1543(m) ν(C=N), 1478(s) ν_{asym}(coordinated NO_3), 1374(vs) ν_{asym}(uncoordinated NO_3), 1339(vs) ν_{sym}(uncoordinated NO_3), 1301(vs), 1275(vs) ν_{sym}(coordinated NO_3), 1208(vs), 1174(m), 1110(w), 1076(m), 1037(vs), 998(vs), 851(m), 828(m), 789(w), 731(s), 683(s).

3.3. X-ray Diffraction Structural Analysis

3.3.1. Structural Analysis of tr_2ad and $tr_2ad{\cdot}3H_2O$

The X-ray diffraction data of tr_2ad (colorless prism with dimensions of 0.27 × 0.22 × 0.20 mm) and $tr_2ad{\cdot}3H_2O$ (colorless prism with dimensions of 0.33 × 0.16 × 0.13 mm) were collected at 173 K on a Bruker APEXII area-detector diffractometer (Bruker, Billerica, MA, USA) equipped with a sealed X-ray tube (Mo-Kα radiation, λ = 0.71073 Å). The data were corrected for Lorentz-polarization effects and for the effects of absorption (multi-scans method). The crystal structures were solved by direct methods and refined against F^2 using the programs SHELXS-97 or SHELXL-2018/1 [54,55]. The non-hydrogen atoms were assigned anisotropic thermal displacement parameters. All the hydrogen atoms were located in difference Fourier maps and then refined freely with isotropic thermal displacement parameters and with soft similarity restraints applied to O–H bond lengths in the structure of $tr_2ad{\cdot}3H_2O$.

Crystal data for tr_2ad, FW = 270.34 g mol^{-1}: monoclinic, $P2_1/n$, a = 8.9372(4) Å, b = 8.7877(5) Å, c = 16.8366(8) Å, β = 97.888(2)°, V = 1309.79(11) $Å^3$, Z = 4, ρ = 1.371 g cm^{-3}, $F(000)$ = 576, $R1$ = 0.039, w$R2$ = 0.095 [$I > 2\sigma(I)$] and $R1$ = 0.053, w$R2$ = 0.1032 (all data) for 2656 data and 253 parameters in the 4.9–52.8° 2θ range. CCDC No. 2034960.

Crystal data for $tr_2ad{\cdot}3H_2O$, FW = 324.39 g mol^{-1}: orthorhombic, *Pnma*, *a* = 9.6759(10) Å, *b* = 16.3052(8) Å, *c* = 10.0229(11) Å, *V* = 1581.3(3) Å^3, *Z* = 4, ρ = 1.363 g cm^{-3}, *F*(000) = 696, *R*1 = 0.049, w*R*2 = 0.087 [$I > 2\sigma(I)$] and *R*1 = 0.110, w*R*2 = 0.104 (all data) for 1656 data and 164 parameters in the 4.8–52.8° 2θ range. CCDC No. 2034961.

3.3.2. Structural Analysis of the Coordination Polymers

Powdered samples (~50 mg) of the five CPs were deposited in the cavity of a silicon free-background sample-holder 0.2 mm deep (Assing S.r.l., Monterotondo, Italy). Powder X-ray diffraction (PXRD) data acquisitions were carried out with a Bruker AXS D8 Advance vertical-scan θ:θ diffractometer (Bruker, Billerica, MA, USA), equipped with a sealed X-ray tube (Cu-Kα, λ = 1.5418 Å), a Bruker Lynxeye linear position-sensitive detector, a filter of nickel in the diffracted beam and the following optical components: primary beam Soller slits (aperture 2.5°), fixed divergence slit (aperture 0.5°), anti-scatter slit (aperture 8 mm). The generator was set at 40 kV and 40 mA. Preliminary PXRD analyses to unveil the purity and crystallinity of the samples were performed in the 2θ range 3.0–35.0°, with steps of 0.02° and time per step of 1 s. PXRD acquisitions for the assessment of the crystal structure were performed in the 2θ range 5.0–105.0°, with steps of 0.02° and time per step of 10 s. After a standard peak search, enabling us to assess the maximum position of the 20–25 lower-angle peaks, indexing was performed applying the Singular Value Decomposition approach [56] implemented in TOPAS-R V3 [57]. The space groups were assigned based on the systematic absences. The crystallographically independent portion of the tr_2ad ligand and nitrate anion were described using rigid bodies built up through the z-matrix formalism, assigning average values to the bond distances and angles (For tr_2ad: $C_{ad/tz}$–C_{ad} = 1.55 Å, C_{tz}–N_{tz}, N_{tz}–N_{tz} = 1.36 Å, C–H = 0.95 Å; Triazole Internal and External Bond Angles = 108 and 126°; Angles at the C_{ad} Atoms = 109.5°. For the Nitrate Anion: N–O = 1.30 Å; O–N–O = 120°.). The structures were solved working in the real space with the Simulated Annealing approach [58], as implemented in TOPAS-R V3. Structures refinement was carried out with the Rietveld method [59], as implemented in TOPAS-R V3. The background was modelled through a polynomial function of the Chebyshev type. An isotropic thermal factor [B_{iso}(M)] was refined for the metal centres; the isotropic thermal factor of lighter atoms was calculated as $B_{iso}(L) = B_{iso}(M) + 2.0$ (Å^2). The peak profile was modelled trough the Fundamental Parameters Approach [60]. The anisotropic shape of the peaks was modelled with the aid of spherical harmonics in all the cases. A correction was applied for preferred orientation adopting the March-Dollase model [61] in the case of $[Zn(tr_2ad)Cl_2]_n$ and $\{[Cu(tr_2ad)(NO_3)](NO_3)\}_n$ (along the [001] pole), as well as of $\{[Cd(tr_2ad)(NO_3)](NO_3){\cdot}H_2O\}_n$ (along the [100] pole). The final Rietveld refinement plots are shown in Figures S5–S9.

Crystal data for $[Zn(tr_2ad)Cl_2]_n$, FW = 406.65 g mol^{-1}: orthorhombic, $P2_12_12_1$, *a* = 14.6240(3) Å, *b* = 10.1054(2) Å, *c* = 11.1204(1) Å, *V* = 1643.40(5) Å^3, *Z* = *Z*′ = 4, ρ = 1.64 g cm^{-3}, *F*(000) = 832.0, R_{Bragg} = 0.051, R_p = 0.057 and R_{wp} = 0.078, for 4801 data and 46 parameters in the 9.0–105.0° 2θ range. CCDC No. 2038425.

Crystal data for $\{[Cu(tr_2ad)Cl]Cl{\cdot}4H_2O\}_n$, FW = 476.91 g mol^{-1}: monoclinic, $P2_1/m$, *a* = 14.5644(9) Å, *b* = 7.1726(4) Å, *c* = 10.9798(6) Å, β = 122.820(3)°, *V* = 963.9(1) Å^3, *Z* = 4, *Z*′ = 2, ρ = 1.64 g cm^{-3}, *F*(000) = 494.0, R_{Bragg} = 0.019, R_p = 0.028 and R_{wp} = 0.040, for 4951 data and 71 parameters in the 6.0–105.0° 2θ range. CCDC No. 2038423.

Crystal data for $[Cd_2(tr_2ad)Cl_4]_n$, FW = 637.00 g mol^{-1}: triclinic, *P*-1, *a* = 6.9425(2) Å, *b* = 12.2352(3) Å, *c* = 12.6513(2) Å, α = 115.621(1)°, β = 90.837(2)°, γ = 101.165(2)°, *V* = 944.74(4) Å^3, *Z* = *Z*′ = 2, ρ = 2.24 g cm^{-3}, *F*(000) = 616.0, R_{Bragg} = 0.050, R_p = 0.049 and R_{wp} = 0.068, for 4901 data and 68 parameters in the 7.0–105.0° 2θ range. CCDC No. 2038421.

Crystal data for $\{[Cu(tr_2ad)(NO_3)](NO_3)\}_n$, FW = 457.95 g mol^{-1}: orthorhombic, *Pnma*, *a* = 7.0648(4) Å, *b* = 10.7226(5) Å, *c* = 22.495(1) Å, *V* = 1704.0(2) Å^3, *Z* = 8, *Z*′ = 4, ρ= 1.79 g cm^{-3}, *F*(000) = 940.0, R_{Bragg} = 0.025, R_p = 0.037 and R_{wp} = 0.048, for 4951 data and 73 parameters in the 6.0–105.0° 2θ range. CCDC No. 2038424.

Crystal data for $\{[Cd(tr_2ad)(NO_3)](NO_3){\cdot}H_2O\}_n$, FW = 524.83 g mol^{-1}: monoclinic, *C*2/*c*, *a* = 23.181(1) Å, *b* = 11. 3867(2) Å, *c* = 15.486(1) Å, β = 108.956(5)°, *V* = 3866.1(3) Å^3, *Z* = *Z*′ = 8,

ρ = 1.80 g cm^{-3}, $F(000)$ = 2112.0, R_{Bragg} = 0.047, R_p = 0.079 and R_{wp} = 0.110, for 4901 data and 53 parameters in the 7.0–105.0° 2θ range. CCDC No. 2038422.

4. Conclusions

In this work, we have described the synthesis and solid-state characterization of the novel coordination polymers (CPs) $[Zn(tr_2ad)Cl_2]_n$, $\{[Cu(tr_2ad)Cl]Cl{\cdot}4H_2O\}_n$, $[Cd_2(tr_2ad)Cl_4]_n$, $\{[Cu(tr_2ad)(NO_3)](NO_3)\}_n$ and $\{[Cd(tr_2ad)(NO_3)](NO_3){\cdot}H_2O\}_n$ [tr_2ad = 1,3-bis(1,2,4-triazol-4-yl)adamantane], isolated as air- and moisture-stable microcrystalline powders by means of solvothermal reactions. As assessed by thermogravimetric analysis, the five CPs show an appreciable thermal stability. As retrieved by powder X-ray diffraction, while $[Zn(tr_2ad)Cl_2]_n$ features 1-D chains, the other compounds contain 2-D double-layers. A comparative structural analysis involving known CPs built up with the tr_2ad ligand unveiled the coordination modes versatility of the ligand and the crystal structure dimensionality variability. Work can be anticipated in the functional characterization of these CPs as heterogeneous catalysts for cutting-edge organic reactions.

Supplementary Materials: The following are available online at http://www.mdpi.com/2304-6740/8/11/60/s1. Detailed synthesis of the tr_2ad ligand (Scheme S1). FTIR spectrum of tr_2ad (Figure S1). Ortep drawings for tr_2ad and $tr_2ad{\cdot}3H_2O$ (Figure S2). Further representation of the crystal structure of $\{[Cu(tr_2ad)Cl]Cl{\cdot}4H_2O\}_n$ (Figure S3). Comparison of bond distances at the metal ion (Figure S4). Graphical result of the final structure refinement carried out on $[Zn(tr_2ad)Cl_2]_n$, $\{[Cu(tr_2ad)Cl]Cl{\cdot}4H_2O\}_n$, $[Cd_2(tr_2ad)Cl_4]_n$, $\{[Cu(tr_2ad)(NO_3)](NO_3)\}_n$, and $\{[Cd(tr_2ad)(NO_3)](NO_3){\cdot}H_2O\}_n$ (Figures S5-S9). The CIF files of tr_2ad, $tr_2ad{\cdot}3H_2O$ and the five CPs, and the checkCIF output files of tr_2ad and $tr_2ad{\cdot}3H_2O$.

Author Contributions: Conceptualization, C.P. and S.G.; investigation: N.X., A.T., S.G., M.M., K.V.D. and G.A.S.; resources: K.V.D., C.P. and S.G.; writing—original draft preparation: A.T. and S.G.; writing—review and editing, A.T. and S.G.; supervision, C.P. and S.G. All authors have read and agreed to the published version of the manuscript.

Funding: This research received no external funding.

Acknowledgments: S.G. acknowledges Università dell'Insubria and C.P. acknowledges Università di Camerino for partial funding.

Conflicts of Interest: The authors declare no conflict of interest.

References

1. Hoskins, B.F.; Robson, R. Infinite polymeric frameworks consisting of three dimensionally linked rod-like segments. *J. Am. Chem. Soc.* **1989**, *111*, 5962–5964.
2. Morsali, A.; Hashemi, L. *Main Group Metal Coordination Polymers: Structures and Nanostructures*; John Wiley & Sons Inc.: Hoboken, NJ, USA, 2017.
3. Patel, V. *Synthesis, Characterization and Application of Coordination Polymers*; Lambert Academic Publishing: Saarbrücken, Germany, 2015.
4. Batten, S.R.; Neville, S.M.; Turner, D.R. *Coordination Polymers: Design, Analysis and Application*; Springer: New York, NY, USA, 2010.
5. Hong, M.-C.; Chen, L. (Eds.) *Design and Construction of Coordination Polymers*; John Wiley & Sons Inc.: Hoboken, NJ, USA, 2009.
6. Yaghi, O.M.; Kalmutzki, M.J.; Diercks, C.S. *Introduction to Reticular Chemistry: Metal-Organic Frameworks and Covalent Organic Frameworks*; Wiley-VCH: Weinheim, Germany, 2019.
7. Kaskel, S. (Ed.) *The Chemistry of Metal-Organic Frameworks: Synthesis, Characterization, and Applications*; Wiley-VCH: Weinheim, Germany, 2016.
8. MacGillivray, L.R.; Lukehart, C.M. (Eds.) *Metal-Organic Framework Materials*; Wiley-VCH: Weinheim, Germany, 2014.
9. Farrusseng, D. (Ed.) *Metal-Organic Frameworks: Applications from Catalysis to Gas Storage*; Wiley-VCH: New York, NY, USA, 2011.
10. Schröder, M. (Ed.) *Functional Metal-Organic Frameworks: Gas Storage, Separation and Catalysis*; Springer: Berlin, Germany, 2010.

11. Li, H.; Wang, K.; Sun, Y.; Lollar, C.T.; Li, J.; Zhou, H.-C. Recent advances in gas storage and separation using metal–organic frameworks. *Mater. Today* **2018**, *21*, 108–121.
12. Rogge, S.M.J.; Bavykina, A.; Hajek, J.; Garcia, H.; Olivos-Suarez, A.I.; Sepúlveda-Escribano, A.; Vimont, A.; Clet, G.; Bazin, P.; Kapteijn, F.; et al. Metal–organic and covalent organic frameworks as single-site catalysts. *Chem. Soc. Rev.* **2017**, *46*, 3134–3184. [PubMed]
13. Kuznetsova, A.; Matveevskaya, V.; Pavlov, D.; Yakunenkov, A.; Potapov, A. Coordination polymers based on highly emissive ligands: Synthesis and functional properties. *Materials* **2020**, *13*, 2699.
14. Heine, J.; Müller-Buschbaum, K. Engineering metal-based luminescence in coordination polymers and metal–organic frameworks. *Chem. Soc. Rev.* **2013**, *42*, 9232–9242. [PubMed]
15. Sun, L.; Campbell, M.G.; Dincă, M. Electrically conductive porous metal–organic frameworks. *Angew. Chem. Int. Ed.* **2016**, *55*, 3566–3579.
16. Mínguez Espallargas, G.; Coronado, E. Magnetic functionalities in MOFs: From the framework to the pore. *Chem. Soc. Rev.* **2018**, *47*, 533–557.
17. Liu, J.-Q.; Luo, Z.-D.; Pan, Y.; Singh, A.K.; Trivedi, M.; Kumar, A. Recent developments in luminescent coordination polymers: Designing strategies, sensing application and theoretical evidences. *Coord. Chem. Rev.* **2020**, *406*, 213145.
18. Zhang, Y.; Yuan, S.; Day, G.; Wang, X.; Yang, X.; Zhou, H.-C. Luminescent sensors based on metal-organic frameworks. *Coord. Chem. Rev.* **2018**, *354*, 28–45.
19. Zhang, X.; Wang, W.; Hu, Z.; Wang, G.; Uvdal, K. Coordination polymers for energy transfer: Preparations, properties, sensing applications, and perspectives. *Coord. Chem. Rev.* **2015**, *284*, 206–235.
20. Wu, M.-X.; Yang, Y.-W. Metal–organic framework (MOF)-based drug/cargo delivery and cancer therapy. *Adv. Mater.* **2017**, *29*, 1606134.
21. Janiak, C.; Vieth, J.K. MOFs, MILs and more: Concepts, properties and applications for porous coordination networks (PCNs). *New J. Chem.* **2010**, *34*, 2366–2388.
22. Robin, A.Y.; Fromm, K.M. Coordination polymer networks with O-and N-donors: What they are, why and how they are made. *Coord. Chem. Rev.* **2006**, *250*, 2127–2157.
23. Kitagawa, S.; Kitaura, R.; Noro, S.-I. Functional porous coordination polymers. *Angew. Chem. Int. Ed.* **2004**, *43*, 2334–2375.
24. Biradha, K.; Sarkar, M.; Rajput, L. Crystal engineering of coordination polymers using 4,4'-bipyridine as a bond between transition metal atoms. *Chem. Commun.* **2006**, 4169–4179. [CrossRef]
25. Gagnon, K.J.; Perry, H.P.; Clearfield, A. Conventional and unconventional metal–organic frameworks based on phosphonate ligands: MOFs and UMOFs. *Chem. Rev.* **2012**, *112*, 1034–1054.
26. Tabacaru, A.; Pettinari, C.; Galli, S. Coordination polymers and metal-organic frameworks built up with poly(tetrazolate) ligands. *Coord. Chem. Rev.* **2018**, *372*, 1–30.
27. Pettinari, C.; Tabacaru, A.; Galli, S. Coordination polymers and metal-organic frameworks based on poly(pyrazole)-containing ligands. *Coord. Chem. Rev.* **2016**, *307*, 1–31.
28. Liao, P.-Q.; He, C.-T.; Zhou, D.-D.; Zhang, J.-P.; Chen, X.-M. Porous Metal Azolate Frameworks. In *The Chemistry of Metal-Organic Frameworks: Synthesis, Characterization, and Applications*; Kaskel, S., Ed.; Wiley: Weinheim, Germany, 2016; Volume 1, pp. 309–343.
29. Liu, K.; Shi, W.; Cheng, P. The coordination chemistry of Zn(II), Cd(II) and Hg(II) complexes with 1,2,4-triazole derivatives. *Dalton Trans.* **2011**, *40*, 8475–8490.
30. Zhang, J.-P.; Zhang, Y.-B.; Lin, J.-B.; Chen, X.-M. Metal azolate frameworks: From crystal engineering to functional materials. *Chem. Rev.* **2012**, *112*, 1001–1033.
31. Pavlov, D.; Sukhikh, T.; Filatov, E.; Potapov, A. Facile synthesis of 3-(azol-1-yl)-1-adamantanecarboxylic acids—New bifunctional angle-shaped building blocks for coordination polymers. *Molecules* **2019**, *24*, 2717.
32. Aromí, G.; Barrios, L.A.; Roubeau, O.; Gamez, P. Triazoles and tetrazoles: Prime ligands to generate remarkable coordination materials. *Coord. Chem. Rev.* **2011**, *255*, 485–546.
33. Beckmann, U.; Brooker, S. Cobalt(II) complexes of pyridazine or triazole containing ligands: Spin-state control. *Coord. Chem. Rev.* **2003**, *245*, 17–29.
34. Klingele, M.H.; Brooker, S. The coordination chemistry of 4-substituted 3,5-di(2-pyridyl)-4*H*-1,2, 4-triazoles and related ligands. *Coord. Chem. Rev.* **2003**, *241*, 119–132.
35. Haasnoot, J.G. Mononuclear, oligonuclear and polynuclear metal coordination compounds with 1,2,4-triazole derivatives as ligands. *Coord. Chem. Rev.* **2000**, *200*, 131–185.

36. Billes, F.; Endrédi, H.; Keresztury, G. Vibrational spectroscopy of triazoles and tetrazole. *J. Mol. Struct. THEOCHEM* **2000**, *530*, 183–200.
37. Nakamoto, K. *Infrared and Raman Spectra of Inorganic and Coordination Compounds*, 6th ed.; Part B; John Wiley & Sons: Hoboken, NJ, USA, 2009.
38. Lever, A.B.P.; Mantovani, E.; Ramaswamy, B.S. Infrared combination frequencies in coordination complexes containing nitrate groups in various coordination environments. A probe for the metal–nitrate interaction. *Can. J. Chem.* **1971**, *49*, 1957–1964.
39. Nakamoto, K. *Infrared and Raman Spectra of Inorganic and Coordination Compounds*, 6th ed.; Part A; John Wiley & Sons: Hoboken, NJ, USA, 2009.
40. Senchyk, G.A.; Lysenko, A.B.; Babaryk, A.A.; Rusanov, E.B.; Krautscheid, H.; Neves, P.; Valente, A.A.; Gonçalves, I.S.; Krämer, K.W.; Liu, S.-X.; et al. Triazolyl–based copper–molybdate hybrids: From composition space diagram to magnetism and catalytic performance. *Inorg. Chem.* **2014**, *53*, 10112–10121.
41. Senchyk, G.A.; Lysenko, A.B.; Rusanov, E.B.; Chernega, A.N.; Jezierska, J.; Domasevitch, K.V.; Ozarowski, A. Structure and magnetic behavior of Cu^{II} MOFs supported by 1,2,4-triazolyl-bifunctionalized adamantane scaffold. *Eur. J. Inorg. Chem.* **2012**, *2012*, 5802–5813.
42. Boldog, I.; Lysenko, A.B.; Rusanov, E.B.; Chernega, A.N.; Domasevitch, K.V. 1,3,5-Triphenyladamantane and 1,3,5,7-tetraphenyladamantane. *Acta Crystallogr. C* **2009**, *65*, o248–o252.
43. Spek, A.L.J. Single-crystal structure validation with the program PLATON. *J. Appl. Crystallogr.* **2003**, *36*, 7–13.
44. Senchyk, G.A.; Lysenko, A.B.; Krautscheid, H.; Sieler, J.; Domasevitch, K.V. A dihydroxidotetracopper(II) framework supported by 4,4′-(adamantane-1,3-diyl)bis(1,2,4-triazole) and benzene-1,3,5-tricarboxylate bridges. *Acta Crystallogr. C* **2008**, *64*, m246–m249.
45. Senchyk, G.A.; Lysenko, A.B.; Krautscheid, H.; Rusanov, E.B.; Chernega, A.N.; Krämer, K.W.; Liu, S.-X.; Decurtins, S.; Domasevitch, K.V. Functionalized adamantane tectons used in the design of mixed-ligand copper(II) 1,2,4-triazolyl/carboxylate metal–organic frameworks. *Inorg. Chem.* **2013**, *52*, 863–872.
46. Senchyk, G.A.; Lysenko, A.B.; Rusanov, E.B.; Chernega, A.N.; Krautscheid, H.; Domasevitch, K.V. Polynuclear and polymeric metal complexes based upon 1,2,4-triazolyl functionalized adamantanes. *Inorg. Chim. Acta* **2009**, *362*, 4439–4448.
47. Senchyk, G.A.; Lysenko, A.B.; Naumov, D.Y.; Fedin, V.P.; Krautscheid, H.; Domasevitch, K.V. Multiple anion···π interactions with a soft selenium atom: Accommodation of $NCSe^-$ anions inside hydrophobic pockets of adamantane/1,2,4-triazole coordination framework. *Inorg. Chem. Commun.* **2010**, *13*, 1576–1579.
48. Senchyk, G.A.; Lysenko, A.B.; Boldog, I.; Rusanov, E.B.; Chernega, A.N.; Krautscheid, H.; Domasevitch, K.V. 1,2,4-Triazole functionalized adamantanes: A new library of polydentate tectons for designing structures of coordination polymers. *Dalton Trans.* **2012**, *41*, 8675–8689.
49. Lysenko, A.B.; Senchyk, G.A.; Lincke, J.; Lässig, D.; Fokin, A.A.; Butova, E.D.; Schreiner, P.R.; Krautscheid, H.; Domasevitch, K.V. Metal oxide-organic frameworks (MOOFs), a new series of coordination hybrids constructed from molybdenum(VI) oxide and bitopic 1,2,4-triazole linkers. *Dalton Trans.* **2010**, *39*, 4223–4231.
50. Lysenko, A.B.; Senchyk, G.A.; Domasevitch, K.V.; Hauser, J.; Fuhrmann, D.; Kobalz, M.; Krautscheid, H.; Neves, P.; Valente, A.A.; Goncalves, I.S. Synthesis and structural elucidation of triazolylmolybdenum(VI) oxide hybrids and their behavior as oxidation catalysts. *Inorg. Chem.* **2015**, *54*, 8327–8338.
51. Senchyk, G.A.; Lysenko, A.B.; Krautscheid, H.; Domasevitch, K.V. Fluoride molecular scissors: A rational construction of new Mo(VI) oxofluorido/1,2,4-triazole MOFs. *Inorg. Chem. Commun.* **2011**, *14*, 1365–1368.
52. Muñoz-Lara, F.J.; Gaspar, A.B.; Muñoz, M.C.; Lysenko, A.B.; Domasevitch, K.V.; Real, J.A. Fast detection of water and organic molecules by a change of color in an iron(II) microporous spin-crossover coordination polymer. *Inorg. Chem.* **2012**, *51*, 13078–13080.
53. Senchyk, G.A.; Bukhan'ko, V.O.; Lysenko, A.B.; Krautscheid, H.; Rusanov, E.B.; Chernega, A.N.; Karbowiak, M.; Domasevitch, K.V. Ag^I/V^V heterobimetallic frameworks generated from novel-type $\{Ag_2(VO_2F_2)_2(triazole)_4\}$ secondary building blocks: A new aspect in the design of SVOF hybrids. *Inorg. Chem.* **2012**, *51*, 8025–8033.
54. Sheldrick, G.M. A short history of SHELX. *Acta Crystallogr. A* **2008**, *64*, 112–122.
55. Sheldrick, G.M. Crystal structure refinement with SHELXL. *Acta Crystallogr. C* **2015**, *71*, 3–8.
56. Coelho, A.A. Indexing of powder diffraction patterns by iterative use of singular value decomposition. *J. Appl. Crystallogr.* **2003**, *36*, 86–95.
57. *Topas-R, V3*; Bruker AXS: Karlsruhe, Germany, 2005.

58. Coelho, A.A. Whole-profile structure solution from powder diffraction data using simulated annealing. *J. Appl. Crystallogr.* **2000**, *33*, 899–908.
59. Rietveld, H.M. A profile refinement method for nuclear and magnetic structures. *J. Appl. Crystallogr.* **1969**, *2*, 65–71.
60. Cheary, R.W.; Coelho, A.A. A fundamental parameters approach to X-ray line-profile fitting. *J. Appl. Crystallogr.* **1992**, *25*, 109–121.
61. Dollase, W.A. Correction of intensities for preferred orientation in powder diffractometry: Application of the March model. *J. Appl. Crystallogr.* **1986**, *19*, 267–272.